Petroleum Science 23 (2026) 5034–5048

Contents lists available at ScienceDirect

Petroleum Science

journal homepage: www.keaipublishing.com/en/journals/petroleum-science

Original Paper

Design and mechanism of side chain-functionalized polysuccinimide for efficient demulsification of crude oil-in-water emulsions at ambient temperature

Xiao-Hong Li [a], Xun Xie [a], Xia Liu [b], Lan Zhou [a], Huan-Jiang Wang [a,*], Can Cui [a], Ya-Dian Xie [a,*]

[a] School of Chemical Engineering, Guizhou Provincial Engineering Research Center for Low-dimensional Materials and Frontier Applications, Guizhou Minzu University, Guiyang, 550025, Guizhou, China
[b] School of Petroleum and Chemical Engineering, Dongying Vocational College, Dongying, 257091, Shandong, China

ARTICLE INFO

Article history:
Received 1 December 2025
Received in revised form
12 May 2026
Accepted 12 May 2026
Available online 17 May 2026

Edited by Yan-Hua Sun

Keywords:
Oil–water separation
Low-temperature demulsifier
Strong polarity
Biodegradable polymer
Dispersion behavior

ABSTRACT

The development of efficient, fast-acting demulsifiers that function effectively at low temperatures is crucial for treating high-water-content crude oil fluids in sustainable oilfield development. In this study, a series of biodegradable and highly polar polyaspartamide-based demulsifiers were synthesized via aminolysis of polysuccinimide (PSI) using aliphatic and aromatic amines. Demulsification tests revealed that PSI modified with phenethylamine (PSI-PEA) exhibited no phase separation capability, even at high dosages and 60.0 °C. In contrast, PSI grafted with 3-dimethylaminopropylamine (PSI-DA) demonstrated excellent low-temperature efficiency, rapidly breaking oil-in-water (O/W) emulsions containing 1.0–10.0 wt% oil. More notably, the co-grafted derivative PSI-PEA-DA showed outstanding versatility and rapid action, achieving up to 99.9% demulsification efficiency for O/W emulsions across a broad pH range (4.0–9.0) and oil content (1.0–20.0 wt%) under ambient conditions within 10 min. Dispersion behavior studies indicated that the aromatic side-chain-modified PSI-PEA tends to form hydrophilic micelles in the aqueous phase, thereby losing its interfacial activity and demulsification capability. Replacement asphaltene experiments, noncovalent interaction (NCI) analysis, and dispersion state microscopy of the co-grafted PSI-PEA-DA demonstrated that the strategic incorporation of aromatic side chains significantly enhances interactions between the demulsifier and natural surfactants. Density functional theory (DFT) calculations further demonstrated that the polyamide backbone of these demulsifiers exhibits stronger polarity than conventional oxygen-based polymers, facilitating stronger binding with the natural surfactants constituting the oil–water interfacial films. Therefore, enhancing polarity and aromaticity of the demulsifier while preserving its structural characteristics represents an effective strategy to reduce the demulsification temperature and improve both the efficiency and speed of demulsification.

1. Introduction

Enhanced oil recovery (EOR) techniques are recognized for their ability to significantly increase crude oil production, often achieving improvements of up to 80.0% compared to conventional primary and secondary recovery techniques (Low et al., 2024; Yonguep et al., 2022). However, the volume of produced fluid has experienced a substantial increase, with levels rising between 300.0% and 500.0% when compared to fluids from primary and secondary recovery processes (Al-Ghouti et al., 2019; Olajire, 2014). More importantly, these produced fluids consist mainly of oil-in-water (O/W) emulsions, which exhibit complex stability, characterized by smaller droplet sizes (1–10.0 μm), higher viscosity, and a water content that often exceeds 90.0% (Deng et al., 2025; Lee et al., 2020). Although scientists and engineers have developed various methods for treating O/W emulsions, these methods

* Corresponding authors.
E-mail addresses: whj2017@gzmu.edu.cn (H.-J. Wang), xieyadian@gzmu.edu.cn (Y.-D. Xie).

Peer review under the responsibility of China University of Petroleum (Beijing).

https://doi.org/10.1016/j.petsci.2026.05.014

include mechanical, thermal, biological, electrical, and chemical approaches (Al-Sakkaf et al., 2024; Raya et al., 2020). However, improving the efficiency of demulsification, along with reducing temperature and shortening processing time is still a challenge for achieving sustainable development and energy conservation in tertiary recovery stages (Husain et al., 2023; Tang et al., 2024).

Chemical demulsification is the most efficient and economical method for treating O/W emulsions and emulsified oily wastewater and can be combined with other techniques (Wang D. et al., 2021; Yan et al., 2024). Thusly, several novel demulsifiers have been developed to tackle harmful O/W emulsions, including modifying commercial reverse demulsifiers such as polyethers and polyamidoamines (Sun et al., 2020; Zhang et al., 2021), nanoparticle-based demulsifiers (Wang et al., 2016), magnetic nanoparticle-based demulsifiers (Yan et al., 2024), bio-based demulsifiers (Mi et al., 2025), and amphiphilic ionic liquids (Hassanshahi et al., 2020). Although some new chemical structure demulsifiers show promise in laboratory tests, they encounter challenges with scalability and cost due to complex manufacturing processes, sensitivity to pH, salinity, temperatures, and the risk of causing environmental contamination. Accordingly, there is still a need to develop efficient, fast, and low temperature demulsifiers to separate O/W emulsions and purify emulsified oily wastewater in the tertiary recovery stages (Ruidas et al., 2022; Yan et al., 2025).

It was widely known that O/W emulsions are stabilized primarily through the adsorption of natural surfactants and chemical flooding agents at the oil–water interface, which facilitates the formation of both rigid interfacial films and electrical double layers around dispersed oil droplets, thereby severely inhibiting droplet coalescence (Sousa et al., 2022; Wang et al., 2017; Zolfaghari et al., 2016). Thusly, an ideal demulsifier should either replace or interact with the native interfacially active species at the oil–water interface and effectively compress the electric double layer surrounding the oil droplets (Huang et al., 2025; Wan et al., 2025). Recently, we proposed improving the aromatic content and polarity of demulsifiers and prepared a series of amphiphilic aromatic poly(amino acid)s, which demonstrate a significant ability to demulsify O/W emulsions with oil concentrations of 1.0–20.0 wt% at room temperature (Wang et al., 2024; Wu et al., 2024; Zhang et al., 2025a). However, analogous to the turbidity effects observed with nonionic demulsifiers (PE/PO), the high-aromatic poly(L-phenylalanine) (PPA) and poly(L-glutamic acid benzyl ester)-*block*-poly(L-phenylalanine) copolymers are prone to aggregation in acidic environments, resulting in a reduction of their surface activity and a diminished capacity for flocculation. Moreover, the synthesis of poly(amino acid)s through ring-opening polymerization (ROP) of amino acid *N*-carboxyanhydride (NCA) precursors remains challenging for industrial-scale implementation due to inherent technical complexities and substantial production costs (Wu et al., 2018). As a result, what strategies can be employed to facilitate the large-scale synthesis of poly(amino acid)-based demulsifiers, and how can their molecular structures be precisely regulated to ensure stability under operational conditions while optimizing their functional efficacy.

As biodegradable and bio-based macromolecules, polysuccinimide (PSI) derivatives possess a poly(amino acid)-like structure and have been used as substitutes for various poly(-amino acid)s in detergents, cosmetics, and medical applications (Chen et al., 2005). More importantly, the synthesis of these polymers via PSI aminolysis presents a highly customizable, cost-effective, and rapid alternative to the conventional production of poly(amino acid)s, which relies on the complex ring-opening polymerization of *N*-carboxyanhydrides (NCAs) (Lam et al., 2023; Wang et al., 2018; Zhang et al., 2017). Herein, we report an innovative design for demulsifiers based on PSI derivatives, leveraging their synthetic simplicity, structural tunability, and inherent biodegradability. Using affordable phenethylamine (PEA) and 3-dimethylaminopropylamine (DMAPA) as modifiers, we prepared a series of PSI derivatives (PSI-PEA, PSI-DA, and PSI-PEA-DA) via aminolysis. Dispersion behavior studies revealed that PSI-PEA, modified solely with an aromatic side chain, tended to form hydrophilic micelles in O/W emulsions, compromising its interfacial activity and demulsification capability. In contrast, PSI-DA, modifing only an alkyl chain, effectively separated 1.0-10.0 wt% O/W emulsions across a wide pH range (4.0–9.0) within 10.0 min at room temperature. Notably, the co-grafted PSI-PEA-DA exhibited superior performance, efficiently treating O/W emulsions with oil contents from 1.0 to 20.0 wt% under the same mild conditions, outperforming PSI-DA. The molecular electrostatic potential (ESP) and molecular polarity index (MPI) analyses indicated that the polyamide backbones of the demulsifiers possess stronger polarity, which enhances the interaction between the demulsifiers and native surfactant molecules that constitute the oil–water interfacial film. Furthermore, competitive adsorption and interaction studies confirmed that it is crucial to incorporate an optimal amount of aromatic side chains, as it significantly boosts the efficiency and versatility of the O/W demulsifiers in complex conditions.

2. Experimental section

2.1. Materials

Polysuccinimide (PSI, molecular weight 7000–8000, RG), 3-dimethylaminopropylamine (DMAPA, RG), phenethylamine (PEA, RG) and triethylamine (Et_3N, >99.5%) were purchased from Macklin Biochemical Co., Ltd. (Shanghai, China). Dimethyl sulfoxide (DMSO, 99.5%), ethyl acetate (EA, 99.5%), petroleum ether (PE, 90–120 °C, >99.5%), anhydrous ethanol (EtOH, >99.5%), heptane, acetone, anhydrous sodium chloride (NaCl, 99.9%), sodium bicarbonate ($NaHCO_3$, 99.9%), and anhydrous calcium chloride ($CaCl_2$, 99.9%) were purchased from Adamas-Beta Bio-Chem Technology Co., Ltd. (Shanghai, China). Sodium hydroxide (NaOH, 99.9%) and hydrochloric acid (HCl) were purchased from Chongqing Chuandong Chemical (Group) Co., Ltd. (Chongqing, China). The crude oil specimen was provided by the China National Offshore Oil Corporation in Tianjin as received. The physical and chemical characteristics as well as the SARA fractions of the oil sample were examined and are detailed in Table S1. The density measured at 25 °C was 0.88 g·cm^{-3}, and the API gravity was approximately 28.3°. The weight percentage composition was quantified as follows: asphaltenes constituted 4.7%, resins accounted for 25.2 %, aromatics comprised 15.2% and saturates represented 48.4%. The deionized water utilized in the study was prepared in the laboratory.

2.2. Demulsifier preparation

The syntheses of PSI derivatives were demonstrated in Fig. 1. PSI-PEA was synthesized by modifying PSI with PEA, where PEA constituted 100% of the succinimide repeating units. Briefly, 0.98 g of PSI (10 mmol of succinimide repeating unit) and 1.20 g of PEA were weighed and added to a three-necked flask. 12.0 mL of DMSO and 3.0 mL of triethylamine were added. The mixture was then heated to 50 °C and stirred for an additional 24 h under a N_2 atmosphere. The resulting PSI-PEA was precipitated and washed with ethyl acetate and acetone using suction filtration. After lyophilization, 2.02 g of a brown derivative was obtained.

The PSI modified solely with DMAPA (100% of succinimide repeating units) was denoted as PSI-DA, while the product modified with PEA (50% of succinimide repeating units) and DMAPA

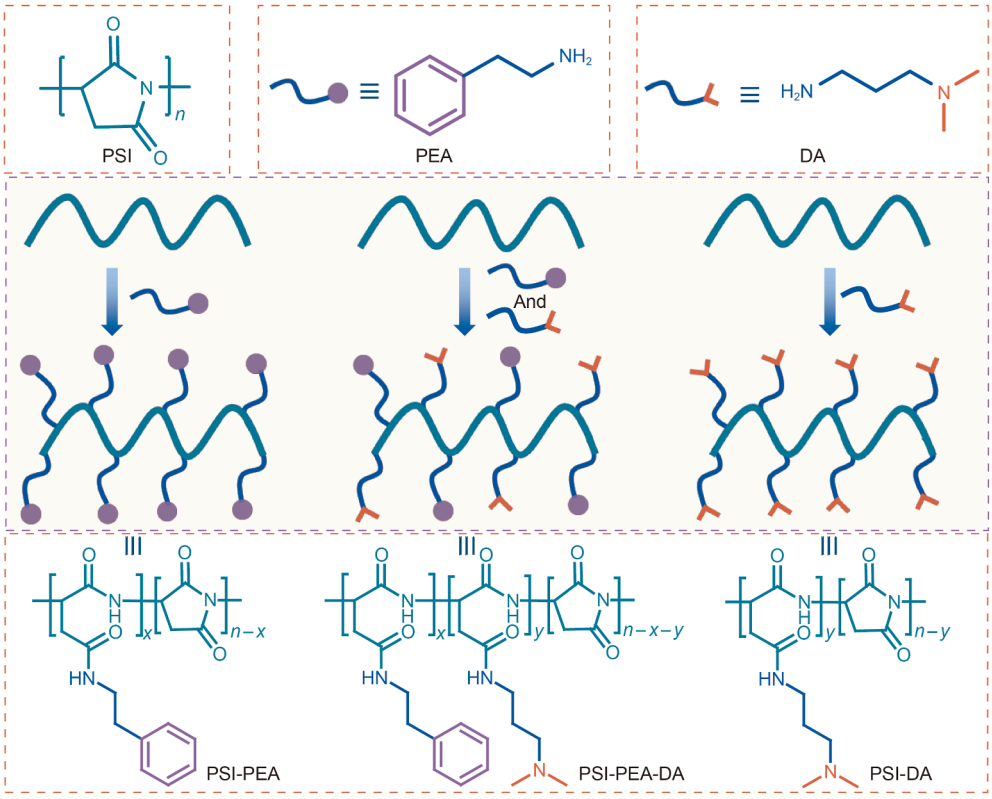

Fig. 1. Synthetic process of the PSI derivative demulsifiers.

(50% of succinimide repeating units) was designated as PSI-PEA-DA. The synthesis of PSI-PEA-DA was similar to that of PSI-PEA, except that two primary amines were used to modify the PSI. Firstly, 0.98 g of PSI and 0.60 g of PEA were weighed and added to a three-necked flask, and 12.0 mL of DMSO and 6.0 mL of triethylamine were added under a N_2 atmosphere. After stirring at 50 °C for 24 h, 0.50 g of DMAPA was added slowly, and the reaction continued for another 24 h. The product was precipitated using ethyl acetate and then washed with acetone. Following freeze-drying, 1.67 g of a light brown powder was obtained.

2.3. Demulsifier characterization

The chemical structures of PSI-PEA, PSI-PEA-DA, and PSI-DA were characterized by a Fourier transform infrared (FT-IR) spectrometer (Nicolet 6700, Thermo Fisher Scientific) in the range of 4000–500 cm^{-1}. The ^1H NMR spectra of the demulsifiers were characterized using an NMR spectrometer (Bruker AVANCE NEO 600M) with DMSO-d_6 as solvent. The molecular weight of the demulsifiers was determined using gel permeation chromatography (GPC) on a Waters GPC 1525 system equipped with a Waters 1525 Isocratic HPLC pump and an Agilent PLgel 5 μm MIXED-C column. Measurements were carried out at a column temperature of 40 °C. DMF containing 1.0 g/L LiBr served as the mobile phase, delivered at a constant flow rate of 1.0 mL/min. Calibration of the system was performed using narrow-dispersity poly(methyl methacrylate) (PMMA) standards.

2.4. Demulsification tests

The emulsified oily wastewater and O/W emulsions were prepared in the laboratory. Briefly, a specific quantity of crude oil and water with varying pH values of 4.0, 6.0, and 9.0 were mixed using a homogenizer (FA 25, Fluko) at 28000 rpm for 5 min. The demulsification performance of the PSI derivative demulsifiers was tested using the bottle method. Briefly, a defined volume of demulsifier ethanol solution with a concentration of 10.0 mg/mL was added to a 15.0 mL emulsion within a colorimeter tube, and the tube was vigorously shaken 200 times. Then, the tubes were placed at ambient temperature without stirring or heating for observing the separation process between water and oil. Following the completion of demulsification, the oil removal efficiency was determined by Eq. (1).

$$E_D = \frac{c_0 - c_i}{c_0} \times 100\% \quad (1)$$

where c_0 and c_i denote the initial and remaining oil concentrations in water, respectively. The detailed evaluation of scale inhibitor performance of PSI derivatives can be found in Supporting Information.

2.5. Revealing the structure–activity relationship of demulsifiers

The impact of demulsifiers' molecular configuration on their interfacial activity was explored through an analysis of their hydrophilic–lipophilic balance (HLB) value and the oil–water tension interface. The theoretical amphiphilicity of demulsifiers was determined by the HLB value (Eq. (2)). The HLB value of non-ionic surfactants is generally between 0 and 20, and high HLB value indicates strong hydrophilicity and vice versa (Griffin, 1954; Wu et al., 2021).

$$HLB = 20(M_a / M_t) \quad (2)$$

where M_a represents the molecular weight of the surfactant molecule's hydrophilic head group; M_t denotes the molecular mass of the complete molecule (Griffin's HLB number).

Interfacial tension of the demulsifiers was measured using a pendant drop method with a contact angle analyzer (CA-100C, Shanghai, China) at room temperature. The oil phase utilized in the interfacial tension experiment consisted of a solution consisting 1:1 mixture of xylene and *n*-heptane. The zeta potentials of O/W emulsions and demulsifiers at various pH values were measured using a Malvern Zetasizer Nano ZS90 to determine the effect of pH on their electrical charge. Each sample was measured ten times to ensure the accuracy of the results.

The ability of PSI derivative demulsifiers to migrate to the oil–water interface and replace/destroy the emulsifiers adsorbed there was investigated. The distribution states of PSI-DA, PSI-PEA-DA, and PSI-PEA in toluene–water and *n*-heptane-water systems, as well as their stability in emulsion formation were examined. The experimental protocol was conducted as follows: a demulsifier dispersion was prepared at a concentration of 0.25 mg/mL. Subsequently, oil samples, specifically heptane and toluene, were introduced into a vial at an oil-to-water volumetric ratio of 1:3. Following the addition of the oil samples, the mixture was subjected to vigorous agitation to monitor the migration behavior of the demulsifiers between the oil and aqueous phases (Wang et al., 2024). The competitive adsorption behavior between the demulsifier and asphaltene at the hydrophilic interface was also studied. Briefly, the new glass slides are washed with xylene, ethanol, and deionized water to eliminate any possible contaminants from their surfaces and dried at 50.0 °C designated as G_0. Next, the clean slides G_0 were soaked in a 100.0 mg/L asphaltene solution for 12 h, then rinsed with xylene and dried at 50.0 °C. The slides coated with a self-assembled layer of asphaltene were designated as G_A. Subsequently, the G_A samples were immersed in PSI-DA and PSI-PEA-DA solutions for 12 h, followed by rinsing with xylene and drying, resulting in competitive adsorption on slides designated as $G_{A\text{-}PD}$ and $G_{A\text{-}PPD}$, respectively. For comparison, the cleaned slides G_0 treated with 100.0 mg/L PSI-DA and PSI-PEA-DA solutions were labeled G_{PD} and G_{PPD}, respectively. These slides when subsequently treated with the asphaltene solution, were labeled $G_{PD\text{-}A}$ and $G_{PPD\text{-}A}$, respectively. Finally, the water contact angle of the modified glass slides was measured to reveal the solubilization and substitution behavior between asphaltenes and demulsifiers at the oil/water interface.

To examine the polarity and aromaticity of demulsifiers and their influence on demulsification efficiency and coagulation capacity, density functional theory (DFT) calculations were conducted utilizing ORCA version 5.0.1 software (Neese et al., 2020). Geometry optimizations were performed employing the BLYP functional with Grimme's long-range dispersion correction (BLYP-D3) in conjunction with Def2-TZVP basis sets. To mitigate basis set superposition error (BSSE), the geometrical counterpoise (gCP) correction method was concurrently applied (Galano et al., 2006). The initial aggregate structure of asphaltene and the model demulsifier was constructed using Molclus (Lu, 2025). The electrostatic potential energy and non-covalent interactions analyses were performed to characterize and visualize the nature of intermolecular interactions within the aggregates using the Multiwfn software package (Lu and Chen, 2012). Furthermore, the interaction strength between asphaltenes, water molecules, and the model demulsifier was quantified by calculating the binding energy (ΔE).

The dispersed state behavior of demulsifiers in an aqueous solution was studied using transmission electron microscopy (TEM) and dynamic light scattering (DLS). To prepare the sample for TEM analysis, a demulsifier solution of DMSO or ethanol at a concentration of 10.0 mg/mL was diluted with pure water to achieve a final concentration of 10.0 mg/L. Subsequently, the prepared samples were then deposited onto an ultra-thin carbon support membrane using a straw and allowed to air dry. Micrographs of PSI-DA, PSI-PEA-DA, and PSI-PEA were obtained using a JEOL JEM-2100 (HR) transmission electron microscope operating at 200 kV. The dispersed state behavior of PSI-DA, PSI-PEA-DA, and PSI-PEA in solution was further analyzed using a Malvern Zetasizer Nano ZS90 instrument at a temperature of 25.0 °C through DLS techniques. The sample preparation procedure for DLS was analogous to that used for the TEM test. Initially, the target demulsifiers were dissolved in DMSO or ethanol to prepare a demulsifier solution with a concentration of 10.0 mg/L. Subsequently, a specific volume of the prepared demulsifier DMSO solution was added to the water, resulting in aqueous dispersions of the demulsifier at concentrations of 10.0 and 100.0 mg/L, respectively. Thereafter, an appropriate amount of the sample was introduced into the cuvet, and the measurement commenced. The entire experiment should be conducted promptly, avoiding any agitation of the samples. The reported data represent the mean values obtained from three independent measurements.

The dispersed oil droplet state in the prepared emulsion, along with the demulsification processes driven by PSI-PEA-DA and PSI-DA, was systematically observed and documented using a polarizing microscope (ZEISS, Axio Scope A1, Germany) to evaluate their coagulation and aggregation capabilities. Briefly, 0.25 mL of the freshly prepared emulsion samples were placed on a clean glass slide and covered with a second slide to facilitate the observation of the dispersion behavior of oil droplets within the aqueous phase. Subsequently, a predetermined volume of demulsifier solution was introduced to 20.0 mL of the O/W emulsion. Following a 5 min equilibration period, a few droplets of the emulsion were carefully extracted and applied to the glass slide to monitor and analyze any subsequent changes in the morphology of the dispersed oil droplets.

3. Results and discussion

3.1. Synthesis and characterization of demulsifiers

To assess the success of the PSI modification, the molecular structures of PSI and its derivatives were analyzed using FT-IR and ^{1}H NMR spectroscopy. As depicted in the FT-IR spectrum of PSI (Fig. 2), the strong characteristic absorption band at 1712 cm^{-1} corresponds to the C=O stretching vibrations, and a small peak at 1792 cm^{-1} is attributed to coupling between two carbonyl groups

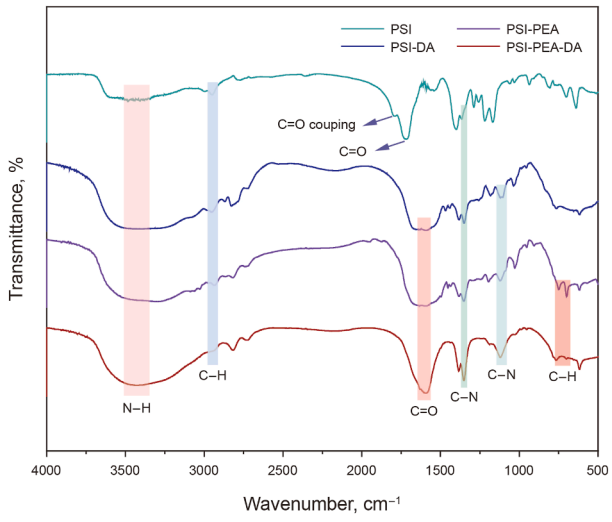

Fig. 2. FT-IR spectra of PSI, PSI-DA, PSI-PEA-DA, and PSI-PEA.

in the five-membered ring of the PSI backbone (Chen et al., 2015; Yeh et al., 2013). The peaks at 3490, 2925, and 1358 cm^{-1} are attributed, respectively, to amide N–H, CH_2, and C–N stretching. In the ^1H NMR spectrum of PSI (Fig. 3(a)), the signals for the methyl and non-equivalent methylene protons in the main chain of PSI appeared at 5.3 ppm (a), 3.2 ppm (b), and 2.7 ppm (b). The results of FT-IR and ^1H NMR all confirmed the presence of the succinimide repeating units in the PSI main chain. Meanwhile, the molecular weight of PSI was determined using GPC to be 7483 g/mol, and the degree of polymerization (the number of succinimide units) of PSI was calculated to be approximately 80 based on the GPC results.

PSI-PEA, PSI-PEA-DA, and PSI-DA were synthesized by aminolysis of the succinimide ring in PSI using PEA and/or DA, which contain hydrophobic aromatic side chain or alkyl side chains. Notably, as shown in Fig. 2, the FT-IR absorption peaks of succinimide ring are nearly absent in the FT-IR spectra of PSI-PEA, PSI-PEA-DA, and PSI-DA. Meanwhile, a distinct absorption peak at 1605 cm^{-1} was observed in each PSI derivative, indicating the formation of new amide bonds through the ring-opening reaction (Cai et al., 2022). Furthermore, the stretching vibration peaks of C–N and N–H in PSI-PEA, PSI-PEA-DA, and PSI-DA at 1358 and 1027 cm^{-1} become more distinct, indicating the introduction of a new primary amine group, which enhances these vibrations (Velazco-de-la-Garza et al., 2020). In both PSI-PEA and PSI-PEA-DA, distinctive C–H stretching vibrations of the benzene ring are detected in the fingerprint region, specifically at 750–700 cm^{-1} (Zhang et al., 2025b).

To further verify the successful synthesis of PSI-PEA, PSI-PEA-DA, and PSI-DA, the structures of target products were determined using ^1H NMR with DMSO-d_6 as the solvent. Fig. 3(b–d) shows that the methine proton signal of the succinimidyl backbone at $\delta = 5.30$ ppm shifts to 4.50 ppm after the aminolysis of PSI units with primary amines, as observed in the ^1H NMR spectra of PSI-PEA, PSI-PEA-DA, and PSI-DA. Meanwhile, the characteristic signals of the side chain primary amine also appeared in the corresponding ^1H NMR spectrum. Specifically, the proton peak attributed to the benzene ring of PEA appeared at $\delta = 7.2$ ppm in ^1H NMR spectra of PSI-PEA (Fig. 3(b)) and PSI-PEA-DA (Fig. 3(c)). The proton peaks corresponding to $–CH_2–$ (g) and $–N(CH_3)_2$ (i) of DMAPA appeared at $\delta = 1.5$ ppm and $\delta = 2.2$ ppm, respectively, in ^1H NMR spectra of PSI-PEA-DA (Fig. 3(c)) and PSI-DA (Fig. 3(d)). FT-IR and ^1H NMR analyses collectively demonstrate the successful

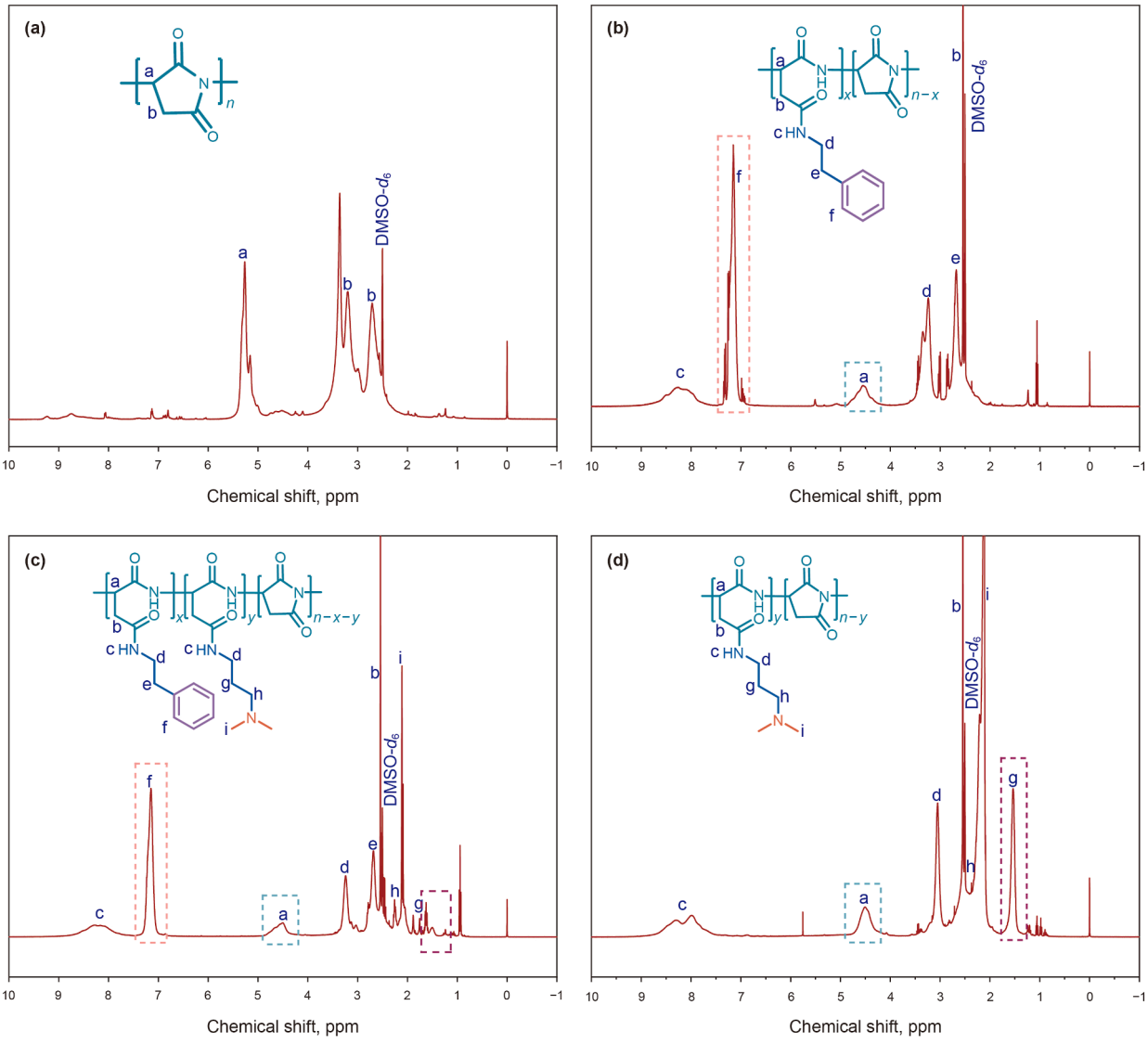

Fig. 3. ^1H NMR spectra of PSI (**a**), PSI-PEA (**b**), PSI-PEA-DA (**c**), and PSI-DA (**d**) in DMSO-d_6.

grafting of hydrophobic side chains onto the PSI backbone via the ring-opening reaction. The degree of substitution (DS) of PSI derivatives by PEA was determined by calculating the integrated area ratio of the signals at 7.2 and 4.5 ppm, which correspond to the benzene ring of PEA and the methine of the succinimide unit. Similarly, the DS of PSI derivatives by DMAPA was determined by analyzing the integrated area ratio of the signals at 1.5 and 4.5 ppm, which correspond to the methine group of DMAPA and of the succinimide unit. The ^{1}H NMR analysis confirmed that the DS values calculated from the spectral data were in close agreement with the initial molar ratios of the primary amines to PSI (Fig. S2). Furthermore, the molecular weights of the synthesized polymers were characterized by GPC, with the results summarized in Table 1 and Fig. S3. The ^{1}H NMR analysis and GPC results indicated that the substitution ratios for the PSI-PEA, PSI-PEA-DA, and PSI-DA samples were approximately 100% (Table 1).

3.2. Demulsifier design and evaluation

3.2.1. Influence of demulsifier structure on demulsification performance

In order to elucidate the correlation between the structure and properties of PSI-PEA, PSI-PEA-DA, and PSI-DA, their demulsification performance was investigated by bottle test. Because PSI-PEA is insoluble in common solvents typically used to dissolve block polyether and polyester demulsifiers, such as ethanol, water, or toluene, a solution of 10.0 mg/mL solution of PSI-PEA in DMSO was prepared prior to conducting demulsification tests. In contrast, PSI-DA and PSI-PEA-DA are soluble in ethanol. Therefore, 10.0 mg/L ethanol solutions of these substances were prepared prior to the demulsification experiment. The demulsification test showed that PSI-PEA was ineffective in separating 5.0 wt% O/W emulsions, even when the demulsifier was added at a concentration of 200.0 mg/L and under operating conditions of 60.0 °C. For comparison, PSI-DA was prepared by modifying PSI solely with DMAPA, while PSI-PEA-DA was prepared by modifying PSI with both PEA and DMAPA at a 1:1 molar ratio. The bottle test experiments demonstrated that both PSI-DA and PSI-PEA-DA effectively separated a 5.0 wt% emulsion under neutral conditions (pH = 6.0) and at ambient temperature. As illustrated in Fig. 4(a) and (b), the optimal dosage of PSI-DA at a concentration of 40.0 mg/L achieved a maximum demulsification efficiency of 99.9%, corresponding to a residual oil content in the separated water of 29.32 mg/L. Notably, PSI-PEA-DA demonstrated superior demulsification performance, achieving an efficiency of nearly 100.0% at a reduced dosage of 10.0 mg/L, yielding a significantly lower residual oil content of 6.10 mg/L in the separated water. Furthermore, PSI-PEA-DA demonstrated faster separation performance for O/W emulsions (Fig. S4) even at this lower dosage. However, it was observed that the demulsification efficiency of PSI-PEA-DA decreases and the remaining oil in the separated water increases when the reagent dosage exceeds the optimal level, indicating that PSI-PEA-DA is more susceptible to reverse emulsification compared to PSI-DA.

Table 1
The molecular weights (M_w), polydispersity index (PDI), degree of substitution (DS), and HLB values of PSI derivatives.

PSI and PSI derivatives	M_w, g/mol	PDI	DS	HLB
PSI	7483	1.92		
PSI-DA	13028	2.18	100	10.02
PSI-PEA-DA	14615	1.97	52:48	8.92
PSI-PEA	15183	2.32	100	7.88

3.2.2. Evaluation of the universality of demulsifiers

The demulsification efficiency and oil removal capacity of the demulsifier are affected by the pH, salinity, and oil concentration of the produced fluid. Consequently, a systematic investigation was conducted to evaluate the impact of these parameters on the oil removal performance of the PSI-DA and PSI-PEA-DA. The experimental findings reveal that both PSI-DA and PSI-PEA-DA exhibit superior oil–water separation performance under acidic (pH = 4.0) and alkaline (pH = 9.0) environments. Specifically, under acidic conditions, the optimal demulsification efficiency of PSI-DA was 99.9% at a dosage of 80.0 mg/L, resulting in a residual oil concentration of 49.92 mg/L in the separated water. In contrast, PSI-PEA-DA achieved a higher maximum demulsification efficiency of 99.9% at a lower dosage of 20.0 mg/L, with the residual oil concentration in the separated water decreasing to 23.86 mg/L (Fig. 4(c)). At a pH of 9.0, the demulsification efficiency of PSI-DA and PSI-PEA-DA both achieved 99.9%. Furthermore, the oil content in the treated water was significantly reduced to 14.85 mg/L for PSI-DA and 10.86 mg/L for PSI-PEA-DA. However, under strongly acidic (pH = 2.0) and strongly basic (pH = 11.0) conditions, both PSI-DA and PSI-PEA-DA lost their efficacy in separating oil and water. It was believed that the protonation of secondary and tertiary amine functionalities in the PSI-DA and PSI-PEA-DA impedes their migration toward the interfacial film (Chen et al., 2019). Furthermore, under highly acidic conditions, the decreased solubility of asphaltenes consequently leads to the formation of a more stable interfacial film (Vafajoo et al., 2012). In a strongly alkaline environment (pH = 11.0), the deprotonation of hydrophilic functional groups in PSI-DA and PSI-PEA-DA further increases the negative charge density around the oil droplets (Lei et al., 2023). This, in turn, intensifies the electrostatic repulsion between the demulsifier molecules and the oil droplets (Ma et al., 2020). As a result, the efficacy of PSI-DA and PSI-PEA-DA in destabilizing O/W emulsions and facilitating phase separation is markedly impaired under highly acidic (pH = 2.0) or highly alkaline (pH = 11.0) environments.

The salt tolerance of the demulsifiers was also evaluated using a 5.0 wt% O/W emulsion prepared with synthetic formation water, the detailed composition of which is provided in Table S2. The bottle test results demonstrated that at the optimal concentration of PSI-DA of 60.0 mg/L, the demulsification efficiency reached 99.9%, and the oil content in the separated water decreased to 31.59 mg/L (Fig. 4(e)). Similarly, at a dosage of 50.0 mg/L, PSI-PEA-DA exhibited a maximum demulsification efficiency of nearly 100.0%, reducing the oil content in the separated water to a minimum of 17.09 mg/L. Compared to the O/W emulsion prepared with deionized water, the O/W emulsion formulated with simulated formation water exhibited a lower residual oil content after separation when treated with the same concentration of demulsifier. This is due to the presence of salt ions in the simulated formation water, which induced a charge shielding effect. This effect attenuated the electrostatic repulsion between emulsified oil droplets, decreased the interfacial tension, and increased the density of the aqueous phase, all of which collectively promotes the demulsification process (Lü et al., 2018; Onaizi, 2022).

At the same time, the deoiling performance of PSI-DA and PSI-PEA-DA for various oil-containing emulsions was investigated. It was found that PSI-DA could only separate 10.0 wt% O/W emulsions at room temperature, but the required settling time was more than 1.5 h. While the PSI-PEA-DA, which contains aromatic side chains, could separate 20.0 wt% O/W emulsions at room temperature within 1 h (Fig. S5). As shown in Fig. 4(g), PSI-DA at a dosage of 50.0 mg/L achieved an optimal demulsification efficiency of nearly 100.0%, corresponding to a residual oil content of 37.69 mg/L in the separated water from 10.0 wt% O/W emulsions.

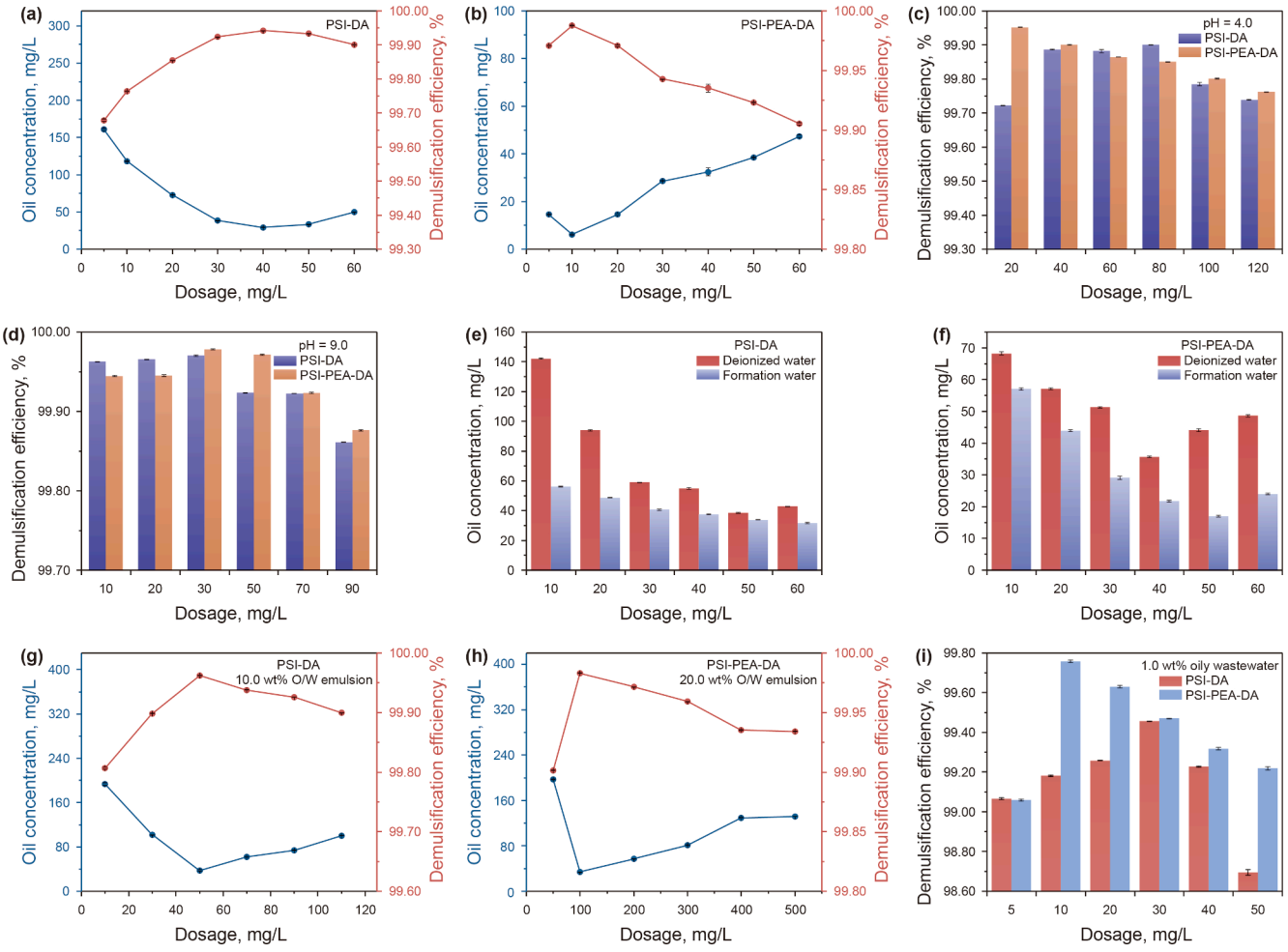

Fig. 4. Influence of various factors on demulsification performance: (**a**, **b**) demulsifier structure; (**c**, **d**) emulsion pH; (**e**, **f**) salinity. (**g**, **h**) Demulsification efficiency of PSI-DA and PSI-PEA-DA at their respective maximum treatable oil contents (10 wt% for PSI-DA, 20 wt% for PSI-PEA-DA). (**i**) Demulsification efficiency of PSI-DA and PSI-PEA-DA for emulsified wastewater with an oil content of 1.0 wt%.

More importantly, PSI-PEA-DA demonstrated optimal demulsification efficiency of nearly 100.0% at a concentration of 100.0 mg/L when applied to the separation of 20.0 wt% emulsions even at room temperature, resulting in a residual oil content as low as 33.68 mg/L. For the treatment of 1.0 wt% oily wastewater, PSI-PEA-DA achieved a superior deoiling efficiency of 99.8% at only 10.0 mg/L, corresponding to a residual oil content of 24.20 mg/L. In comparison, PSI-DA required a higher dosage of 30.0 mg/L to reach an efficiency of 99.5%, yielding a residual oil of 54.43 mg/L. The evaluation of PSI-DA and PSI-PEA-DA confirmed that the strategic incorporation of aromatic groups significantly enhanced demulsification performance, enabling PSI-PEA-DA to rapidly separate O/W emulsions with elevated oil content at room temperature. Furthermore, benchmarking against commercial polyamide amine demulsifiers (KZ-5, K-122) from the target oilfield was conducted. As shown in Fig. S6, the commercial demulsifiers failed to separate the emulsion at ambient temperature. In contrast, PSI-PEA-DA, featuring aromatic side chains and a newly formed polar backbone, achieved rapid and efficient demulsification at lower temperatures. The enhanced demulsification performance of PSI-PEA-DA directly validates that increasing molecular polarity and aromaticity is a viable strategy for developing novel, high-efficiency demulsifiers for low-temperature applications.

3.3. Exploration of the demulsification mechanism

3.3.1. Interfacial properties and zeta potential of demulsifiers

Since PSI-PEA, PSI-PEA-DA, and PSI-DA contain hydrophilic polyamide backbones and hydrophobic side chains, they can be considered as a class of macromolecular surfactants. Therefore, we calculated their HLB values based on ^{1}H NMR and GPC results. The HLB value was determined by the types and quantities of hydrophilic and lipophilic components within the demulsifier molecules, as shown in Table 1. Within the molecular structure, PEA contributes a hydrophobic domain, whereas DA functions as the hydrophilic component. As presented in Table 1, the incorporation of DA side chains into PSI-PEA led to a consistent increase in the HLB, with values incrementally rising from 7.88 for PSI-PEA to 8.92 for PSI-PEA-DA. It is well known that HLB is a parameter used to describe the balance between the hydrophilic (water-attracting) and lipophilic (oil-attracting) portions of surfactants (Li et al., 2018). Therefore, PSI-PEA with the lowest HLB, demonstrated a pronounced tendency to migrate to the oil droplet surface and exhibited the highest surface activity in reducing the oil–water interfacial tension. For comparison, the interfacial tension measurements were performed to investigate the interfacial activity of the PSI-PEA, PSI-PEA-DA, PSI-DA, and polymers using the pendant-

drop method. However, in contrast to the anticipated HLB value, PSI-PEA did not result in a notable reduction in the interfacial tension between heptane/xylene and water, even when used at a concentration of 110.0 mg/L (Fig. 5(a)). The loss of interfacial activity in PSI-PEA, demonstrated by its inability to migrate to and reduce tension at the oil–water interface, is likely due to a structural rearrangement in aqueous environments. This phenomenon can be attributed to the structural composition of PSI-PEA, in which the polymer backbone consists of a hydrophilic polyamide formed by ammonolysis, while the pendant side chains contain hydrophobic aromatic moieties. Upon introduction into an aqueous environment, the hydrophobic side chains tend to aggregate, forming a hydrophobic core stabilized by π–π interactions among the benzyl groups. Meanwhile, the hydrophilic polyamide backbone reorganizes to form the outer shell of the micellar structures (Wang et al., 2024). The studies of the migration, emulsification stability, dispersion state, and coagulation ability of PEA in the mechanism exploration section further confirm the validity of this hypothesis.

However, PSI-PEA-DA and PSI-DA could effectively decrease the interfacial tensions between oil and water to 31.4 and 36.6 mN/m, respectively, under neutral conditions at their optimal concentrations. Specifically, at a pH of 4.0, the interfacial tension values for PSI-PEA-DA and PSI-DA were 41.0 and 36.9 mN/m, respectively. Notably, under alkaline conditions (pH = 11.0), the tensions decreased further to 30.8 mN/m for PSI-PEA-DA and 34.8 mN/m for PSI-DA. These findings suggest that PSI-PEA-DA and PSI-DA are capable of migrating to the oil–water interface and interacting with the interfacial film after added into emulsions. However, demulsification tests showed that PSI-PEA-TA and PSI-TA did not promote the separation of O/W emulsions at a pH of 11.0. It is well established that the zeta potential of the demulsifier aqueous dispersions can be used as a powerful method to investigate the pH-dependent electrochemical behavior influencing the initial interactions with charged emulsion droplets during demulsification (Mi et al., 2025). Thus, the influence of aqueous phase pH on the zeta potential of the emulsions and demulsifiers (PSI-PEA-DA, PSI-DA) was therefore investigated. As shown in Fig. 5(d), at a pH of 11.0, the zeta potential of both the demulsifiers and the emulsion droplets was below −30.0 mV. These highly negative values of demulsifiers and the emulsion droplets not only increased the stability of the emulsion but also promoted electrostatic repulsion between them, thereby enhancing stability through both steric and electrostatic effects. Consequently, although the demulsifiers can migrate to the oil−water interface, this electrostatic repulsion prevents them from effectively compressing the electrical double layer, disrupting the rigid interfacial film, or ultimately achieving phase separation at room temperature.

3.3.2. *Migration ability and replacement of asphaltenes by demulsifiers*

Generally, the efficacy of a demulsifier critically depends on its ability to migrate to the oil–water interface and disrupt the stabilizing interfacial film by competitively displacing the original stabilizing agents (Yang et al., 2025). Thusly, we investigated the migration and emulsion stabilization capacity of PSI-DA, PSI-PEA-DA, and PSI-PEA in both toluene–water and *n*-heptane–water systems. As demonstrated in Fig. 6(b) and (d), PSI-PEA was unable to stabilize emulsions in both toluene–water and *n*-heptane–water systems, exhibiting a tendency to remain dispersed within the aqueous phase rather than migrating to the oil–water interface. These results further demonstrate that the structural configuration of PSI-PEA undergoes a transformation upon exposure to the aqueous phase, resulting in newly formed hydrophilic particles

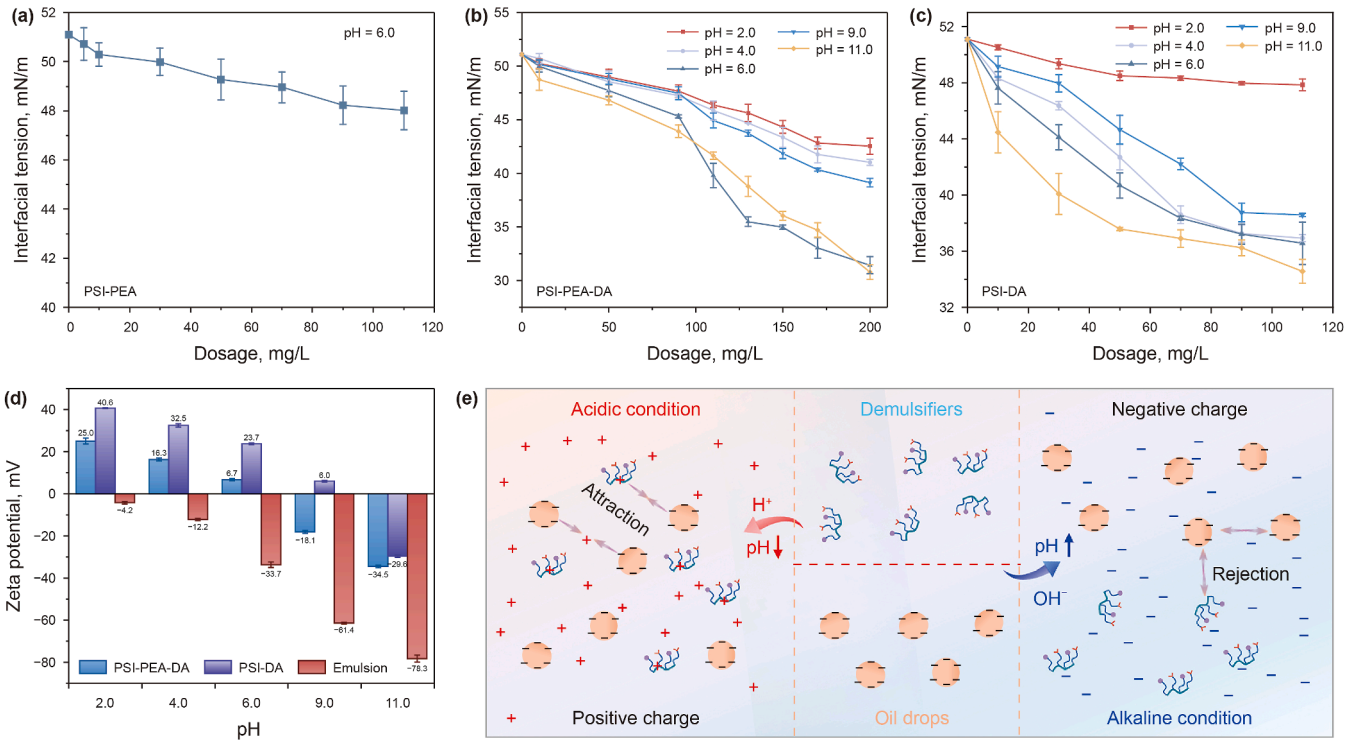

Fig. 5. Interfacial tension of the demulsifiers as a function of concentration under different pH conditions: (**a**) PSI-PEA; (**b**) PSI-PEA-DA; (**c**) PSI-DA. (**d**) Zeta potential of the demulsifiers and O/W emulsions under varying pH conditions. (**e**) Schematic diagram illustrating the interactions between the demulsifiers and O/W emulsions at different pH values.

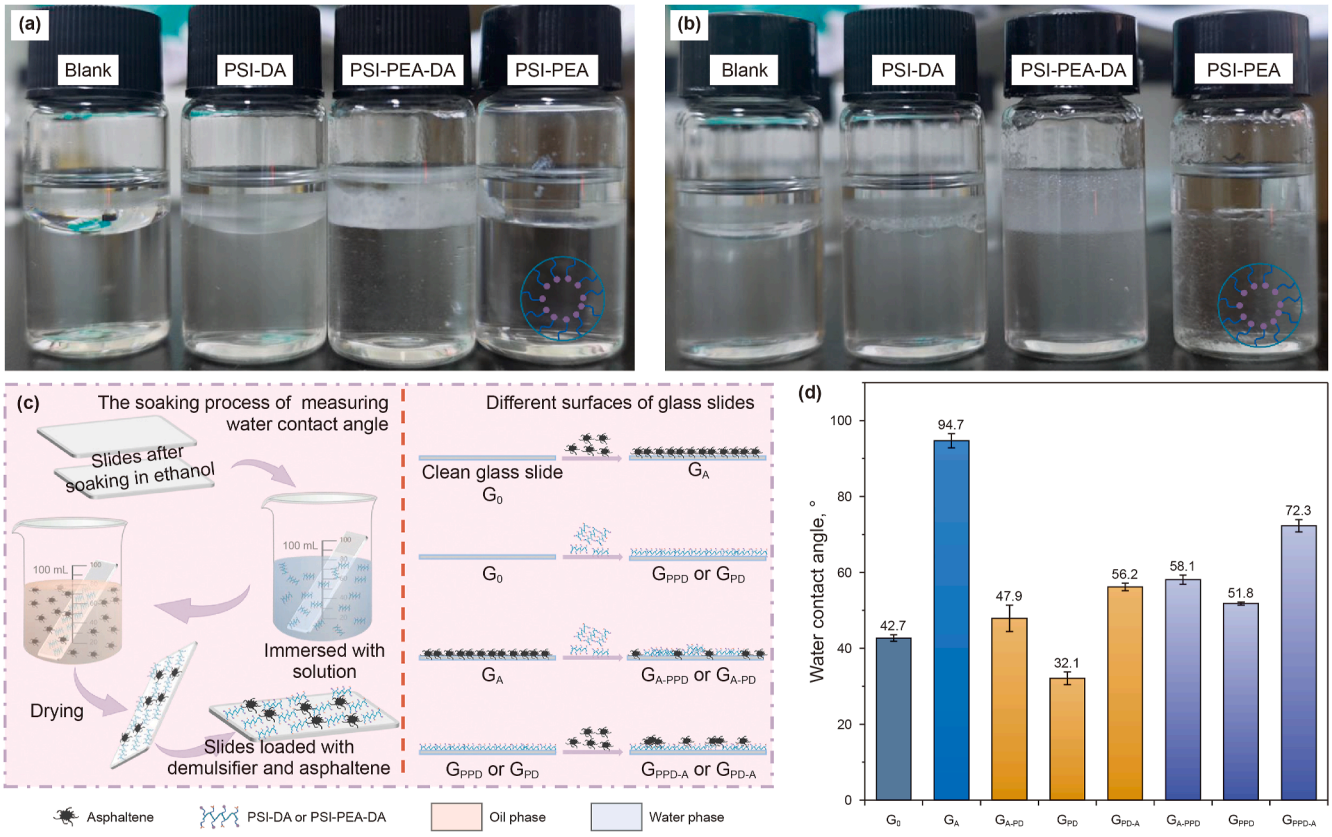

Fig. 6. The ability of PSI-DA, PSI-PEA-DA, and PSI-PEA to stabilize O/W emulsions: (**a**) toluene–water system; (**b**) *n*-heptane–water system; (**c**) schematic of replacement of asphaltene molecules onto the surface of a glass slide by demulsifier; (**d**) water contact angles of the glass slide surfaces after treatment.

with a hydrophobic core and hydrophilic outer shell. Notably, PSI-DA consists solely of alkyl side chains and is less effective at stabilizing these emulsions. However, it can migrate to the oil–water interface and form an observable interfacial film. In contrast, PSI-PEA-DA, which contains both aromatic and alkyl side chains, effectively stabilizes emulsions in both toluene–water and *n*-heptane–water systems.

The capacity of demulsifiers to solubilize asphaltene films was investigated using water contact angle (WCA) measurements, which reveal the ability of a demulsifier to displace asphaltenes from the oil–water interface (Yu et al., 2024). As illustrated in Fig. 6(c) and (d), a pristine glass slide (G_0) exhibited a WCA of 42.7°, confirming its hydrophilicity. After immersion in an asphaltene solution, the WCA of the resulting surface (G_A) increased to 94.7°, indicating successful adsorption of asphaltenes, which rendered the surface hydrophobic. In contrast, surfaces pre-coated with PSI-DA (G_{PD}) and PSI-PEA-DA (G_{PPD}) showed lower WCAs of 32.1° and 51.8°, respectively, demonstrating their hydrophilic nature. More importantly, when the asphaltene-coated G_A was subsequently immersed in demulsifier solutions, the WCAs decreased to 47.9° ($G_{A\text{-}PD}$, treated with PSI-DA) and 58.1° ($G_{A\text{-}PPD}$, treated with PSI-PEA-DA). Conversely, when demulsifier-coated slides (G_{PD} and G_{PPD}) were exposed to asphaltenes, the WCAs increased to 56.2° ($G_{PD\text{-}A}$) and 72.3° ($G_{PPD\text{-}A}$). This finding provides further evidence that both demulsifiers can displace pre-adsorbed asphaltenes from the slide surface, whereas asphaltenes cannot displace demulsifiers that have been previously adsorbed. Concurrently, due to the inherent concentration gradient of asphaltenes, a certain amount of asphaltenes was adsorbed onto the glass surface, resulting in an increase in the WCA of $G_{PD\text{-}A}$ and $G_{PPD\text{-}A}$ (Shen et al., 2024).

Notably, the WCAs on the glass slides $G_{A\text{-}PD}$ and $G_{A\text{-}PPD}$ are marginally lower than $G_{PD\text{-}A}$ and $G_{PPD\text{-}A}$, yet significantly lower than on G_A. These changes indicated that asphaltene molecules exhibit limited capability to displace PSI-DA and PSI-PEA-DA molecules adsorbed on the glass slide surface. On the contrary, the demulsifier PSI-DA and PSI-PEA-DA are more capable of solubilizing and replacing the asphaltene molecules on the glass slide. More importantly, the WCA gap between G_{PPD} and $G_{A\text{-}PPD}$ was only 6.3°, which is smaller than the 15.8° gap between G_{PD} and $G_{A\text{-}PD}$, indicating that PSI-PEA-DA molecules exhibit superior capability to displace asphaltene molecules adsorbed on the glass slide surface compared to PSI-DA molecules. The competitive adsorption results confirm that incorporating aromatic side chains into PSI-DA enhances its ability to disrupt and replace the rigid oil–water interfacial film. Consequently, PSI-PEA-DA achieves a significantly higher demulsification rate, along with improved efficiency and versatility, particularly at low temperatures.

3.3.3. *Polarity and aromaticity of the demulsifiers*

The ESP is a well-established descriptor for visualizing charge distribution and predicting intermolecular interactions (Lu, 2024). In O/W emulsions, stability is largely attributed to asphaltenes, resins, and other native surfactants, which associate via H-bonding, δ–δ, δ–π, and π–π stacking interactions. Among these, π–π stacking serves as the principal driving force for the formation of the oil–water interfacial film, thereby inhibiting oil droplet

coalescence (Ma et al., 2021; Wang, D. et al., 2021). To evaluate how demulsifier polarity disrupts this network, we analyzed the ESP of the polyamide and polyester backbones of the demulsifiers. The ESP mapped onto the van der Waals (vdW) surfaces of polyamide and polyester is presented in Fig. 7(a) and (b), with cyan and orange spheres denoting the respective minima and maxima. As shown in Fig. 7(a), the polyamide backbone exhibits its most negative ESP regions (minima) around the lone pairs of the amide oxygen atoms, with a surface minimum of −45.02 kcal/mol. The maximum positive ESP reaches 50.59 kcal/mol. In contrast, the polyester (Fig. 7(b)) shows its primary negative ESP around the ester oxygen lone pairs, with a less negative minimum of −37.79 kcal/mol and a lower positive maximum of 42.14 kcal/mol. The polarity was further quantified by the MPI (Liu et al., 2021), which yielded values of 16.85 kcal/mol for polyamide and 14.95 kcal/mol for polyester. The elevated MPI of polyamide confirms its greater overall polarity. This conclusion is corroborated by the area distribution statistics of the ESP over the van der Waals surface (Fig. 7(c)), which reveals a broader ESP distribution for polyamide compared to the relatively confined range for polyester. Analysis of the polarity of the main chain indicates that the polyamide backbone has a superior capacity to interact with native surfactant molecules compared to its polyester counterpart.

Building on the established understanding that the polyamide backbone ($\Delta E_{\text{Y-PA}} = -29.88$ kcal/mol) interacts more strongly with asphaltenes than the polyether backbone ($\Delta E_{\text{Y-PE}} = -28.51$ kcal/mol) (Wang et al., 2024), the interactions between PSI-PEA-DA and asphaltene (Yen model) was investigated. Fig. 7(d) and (e) depicts the packing model and nature of the interaction between PSI-PEA-DA and asphaltene molecules. The colors on a blue-green-red (BGR) scale range from −0.005 to 0.005 a.u. As given in independent gradient model based on Hirshfeld partition (IGMH) isosurfaces of their dimers (Fig. 7(d)), a series of large discontinuous green isosurfaces are observed between the polyamide backbone of PSI-PEA-DA and the hydrophobic conjugated systems and alkyl chains of the asphaltene molecules. These features indicate the presence of hydrogen bonding interactions, specifically CH···N and C=O···H, as well as lone pair−π interactions involving C=O···π. Notably, the backbone of PSI-PEA-DA exhibits a preferential interaction with asphaltene molecules over the alkyl and aromatic side chains. This selectivity is attributed to the greater strength of n–π interactions compared to π–π and/or π–σ interactions (Hao et al., 2021; Mooibroek et al., 2008).

Since both polymers share the same primary polyamide architecture, the enhanced versatility and superior asphaltene displacement capability of PSI-PEA-DA and PSI-DA must originate from their side chains. Therefore, the interaction strength between the distinct side-chain functional groups of PSI-PEA-DA/PSI-DA and Yen model was investigated to elucidate the origin of their performance gap. For the DA–asphaltene dimer (Fig. 7(f)), only a small, discrete green isosurface is observed, indicating a weak π–δ interaction. In contrast, the PEA–asphaltene dimer (Fig. 7(g)) exhibits a considerably larger green isosurface, signifying the presence of both π–δ and π–π interactions. Furthermore, the binding energies ($\Delta E_{\text{P-A}} = -17.46$ kcal/mol) observed between asphaltene and PEA are markedly higher than those between asphaltene and

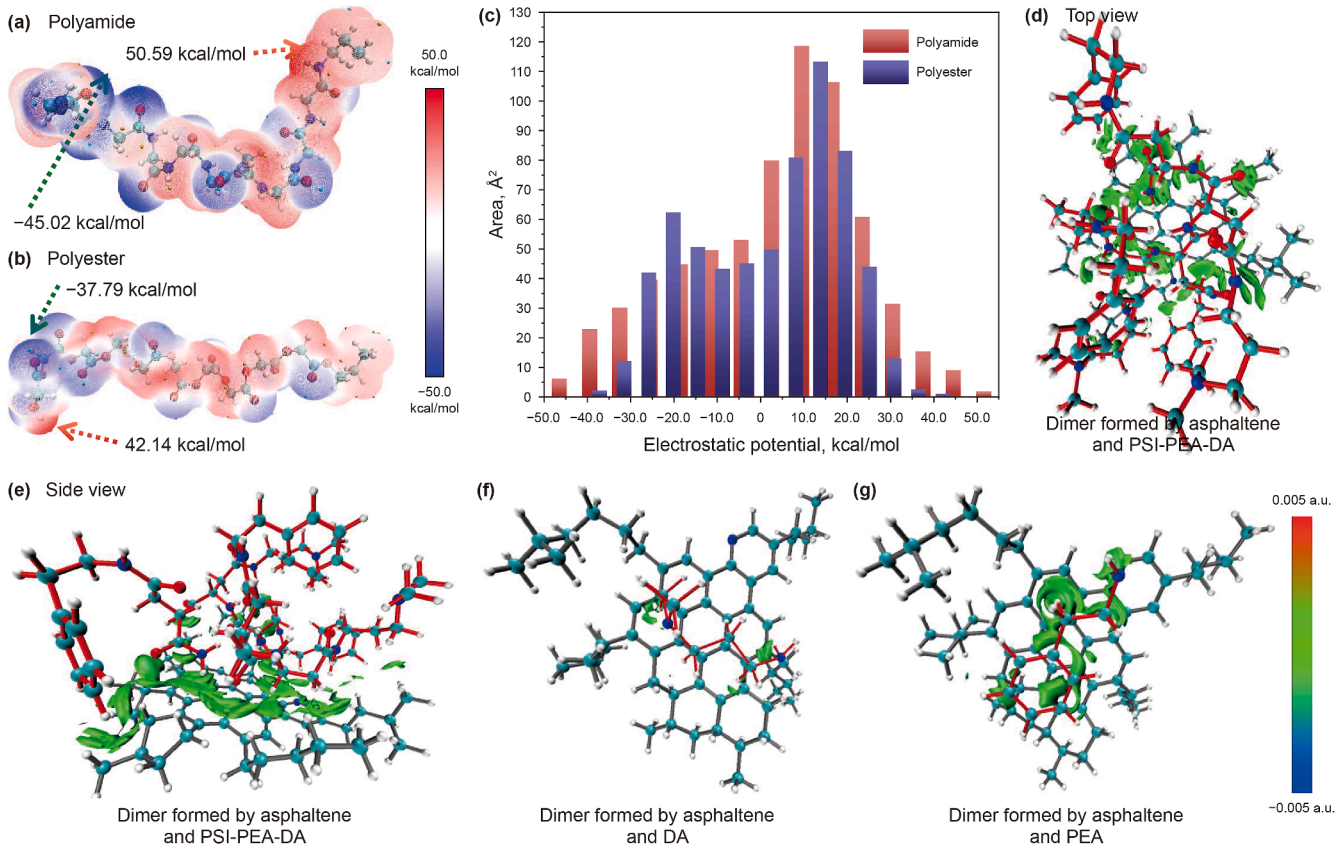

Fig. 7. ESP color mapped onto the electron density isosurface ($\rho = 0.001$ a.u.) of polyamide (**a**) and polyester (**b**). (**c**) Area on the isosurface within different ESP ranges for polyamide and polyester. IGMH maps of dimers formed by asphaltene and PSI-PEA-DA: (**d**) top view; (**e**) side view. IGMH maps of dimers formed by asphaltene and DA (**f**), and asphaltene and PEA (**g**).

DA ($\Delta E_{D\text{-}A} = -15.22$ kcal/mol), confirming that the aromatic PEA side chain engages in more interactions with asphaltene. The findings from the IGMH analysis indicate that the aromatic region and the highly polar polyamide framework of PSI-PEA-DA facilitate the adsorption of asphaltene molecules through van der Waals interactions and hydrogen bonding. This interaction potentially contributes to the disruption of nanoaggregates or clusters composed of asphaltenes, resins, and other substances that form interfacial films at the oil–water interface. However, the reported conventional O/W demulsifiers, despite incorporating aromatic functional groups, fail to demonstrate effective demulsification at ambient temperature (Kuang et al., 2019). Therefore, we propose that the stronger polarity of the polyamide backbone in these demulsifiers enables them to effectively separate O/W emulsions under low-temperature conditions. Moreover, the incorporation of the aromatic side chain has improved the demulsification performance and expanded the functional scope of PSI-PEA-DA.

3.3.4. Dispersion status and coagulation capability of demulsifiers

The assessment of interfacial tension and dispersion migration capacity revealed that the dispersion state of PSI-PEA changed upon its introduction into the aqueous phase. Consequently, DLS and TEM were employed to investigate the aggregation behavior of PSI-DA, PSI-PEA-DA, and PSI-PEA in an aqueous medium. As shown in Fig. 8(a–c), TEM imaging revealed that at a low concentration (10.0 mg/L), PSI-PEA self-assembled into small spherical nanoparticles approximately 3.8 nm in diameter. PSI-DA, however, formed an irregular film on the copper substrate, while PSI-PEA-DA exhibited a characteristic flocculated morphology.

Furthermore, DLS analysis (Fig. 8(d)–(f) and Table S3) revealed that the aggregate characteristics of PSI-PEA show little dependence on concentration. The hydrodynamic diameter (D_h) remained virtually unchanged, measuring 159.5 nm at 10.0 mg/L and 164.2 nm at 100.0 mg/L, with correspondingly low and stable PDI values (0.369 and 0.396). This minimal variation confirms that PSI-PEA tends to form stable, uniform nanoparticles in aqueous media, and its dispersion state is not significantly perturbed by increasing concentration.

Collectively, the studies of interfacial tension, migration ability, and existence state demonstrate that PSI-PEA undergoes spontaneous self-assembly into nanoparticles in the aqueous phase. This structural alteration compromises interfacial activity of PSI-PEA and explains its inability to separate O/W emulsions, even at high concentrations. In contrast, PSI-PEA-DA and PSI-DA exhibit concentration-dependent aggregation in water, as evidenced by significant changes in D_h and PDI. Unlike the defined nanoparticles of PSI-PEA, PSI-PEA-DA forms larger, irregular aggregates, which is consistent with its effective demulsification performance. Moreover, the incorporation of alkyl side chains in PSI-PEA-DA disrupts the π–π stacking between aromatic rings, thereby suppressing the formation of compact self-assemblies of PSI-PEA-DA through both intermolecular and intramolecular interactions in aqueous media.

To directly compare the flocculation capabilities of PSI-DA and PSI-PEA-DA, we employed polarizing optical microscopy (POM) to track oil droplet dynamics after their addition to a 5.0 wt% O/W emulsion at their optimal dosages. Samples taken after 5 min of settling revealed that both demulsifiers induced significant droplet aggregation, forming irregular oil clusters. However, the flocs formed in the PSI-PEA-DA-treated emulsion (Fig. 9(c)) were visibly larger and

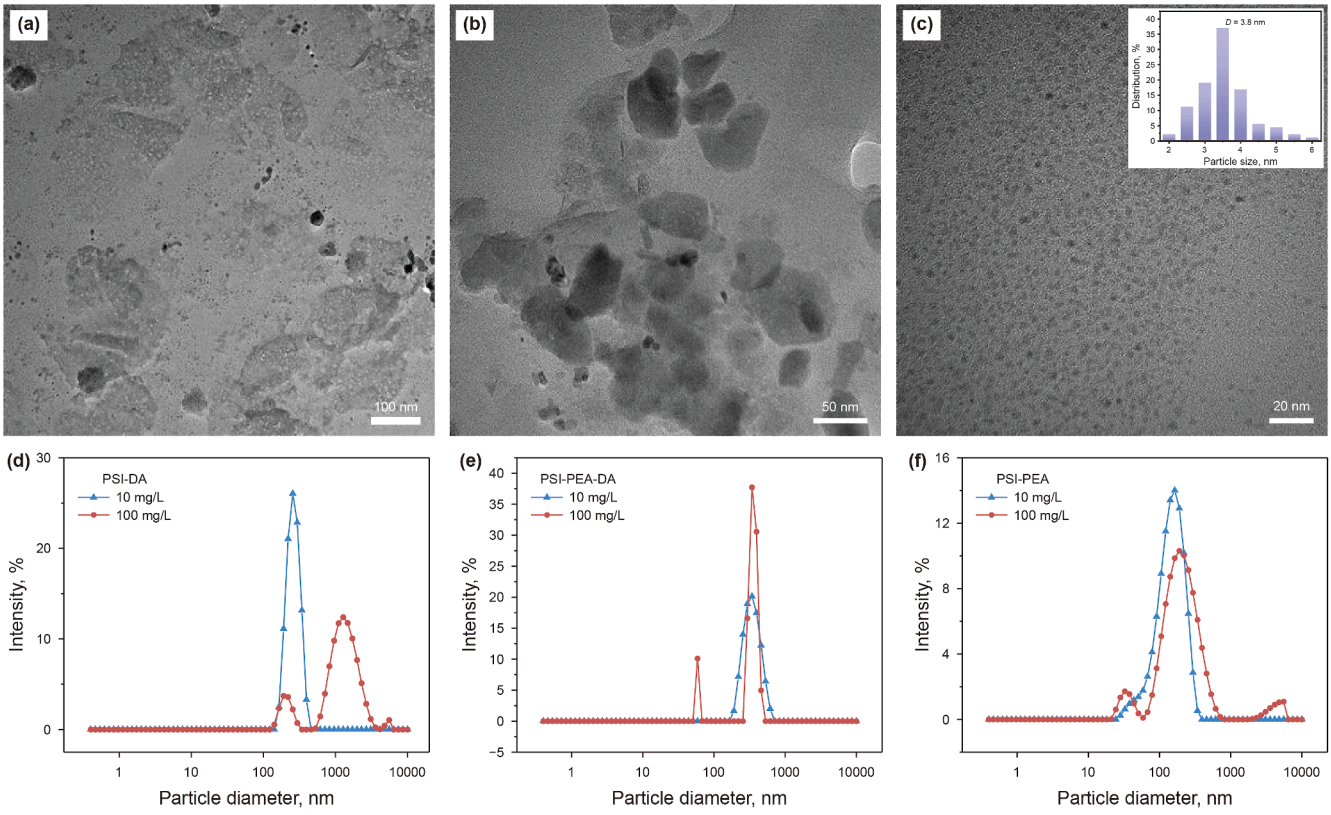

Fig. 8. TEM images of the dispersed forms of PSI-DA (**a**), PSI-PEA-DA (**b**), and PSI-PEA (**c**) in the aqueous phase. Hydrodynamic diameter (D_h) distributions of the aggregates formed in the aqueous solutions of PSI-DA (**d**), PSI-PEA-DA (**e**), and PSI-PEA (**f**) at 298.15 K.

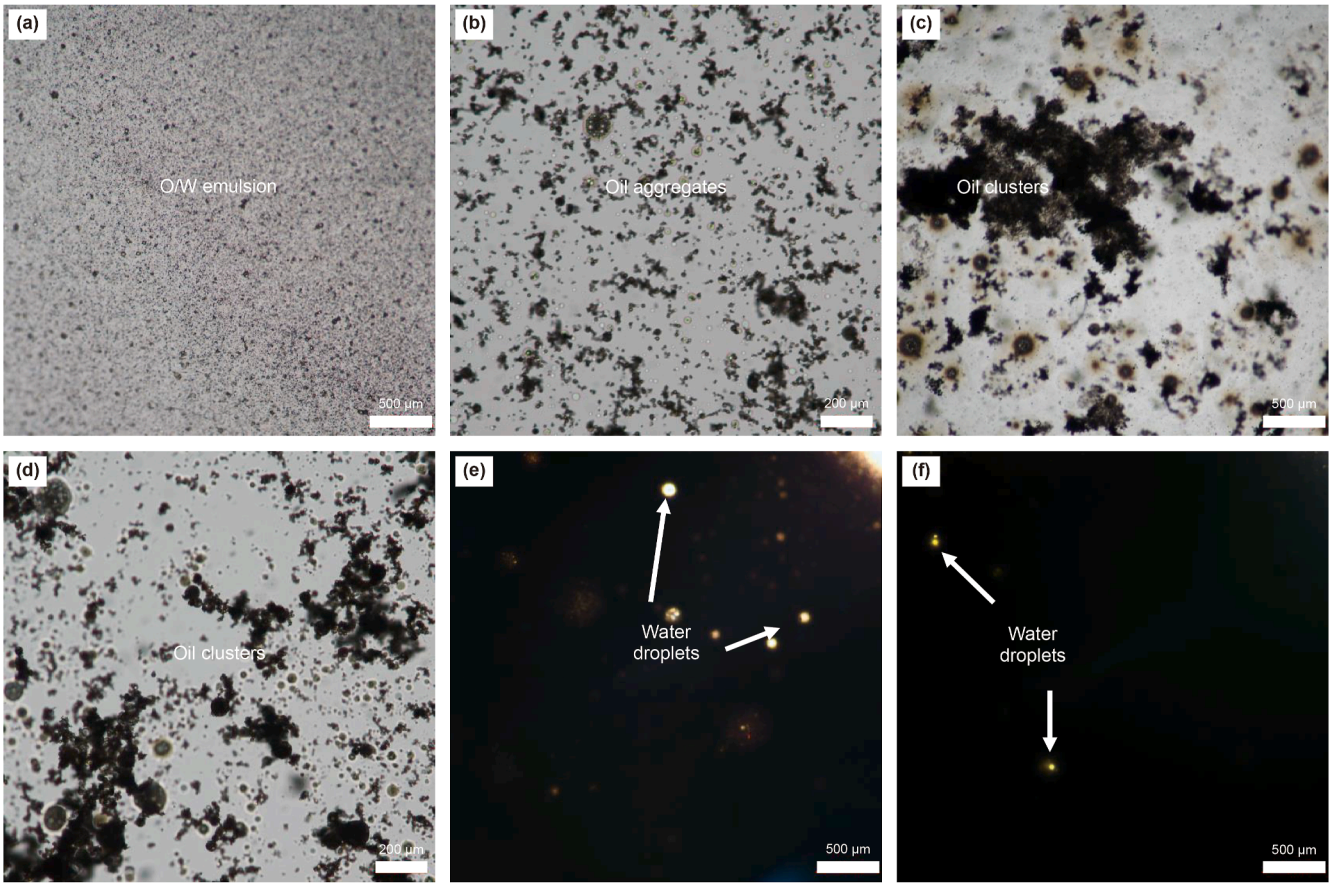

Fig. 9. Microscopic images of the O/W emulsions before and after treatment with PSI-DA and PSI-PEA-DA: (**a**) freshly prepared emulsion; (**b**) emulsion after treatment with PSI-DA for 5.0 min; (**c**) emulsion after treatment with PSI-PEA-DA for 5.0 min, (**d**) emulsion after treatment with PSI-DA for 10.0 min; (**e**) newly formed oil phase after treatment with PSI-DA and standing for 1 h; (**f**) oil phase after treatment with PSI-PEA-DA and standing for 1.0 h.

more densely packed than those in the PSI-DA-treated system (Fig. 9(b)). This striking difference in floc size provides direct visual evidence that PSI-PEA-DA possesses a markedly superior flocculation capacity compared to PSI-DA, corroborating its enhanced oil removal efficiency and universality. Furthermore, the deep dehydration efficacy of PSI-PEA-DA and PSI-DA was evaluated. After demulsification and 1.0 h of settling, the separated oil phase was analyzed. As shown in Fig. 9(e) and (f), the oil phase treated with PSI-DA contained some residual water droplets, whereas the sample treated with PSI-PEA-DA showed a markedly lower number of droplets. This visual observation was confirmed by water content analysis, which measured only 0.28% in the oil phase treated with PSI-PEA-DA. These results demonstrate that the incorporation of aromatic side chains significantly enhances the flocculation and deep dehydration capabilities of PSI-PEA-DA.

Based on comprehensive demulsification tests and mechanistic analyses, we propose a demulsification mechanism for PSI-PEA-DA, as illustrated in Fig. 10. Upon addition to an O/W emulsion, the demulsifier rapidly migrates to the oil–water interface, driven by its balanced amphiphilicity and high interfacial activity (Fig. 10(a) and (b)). Subsequently, the synergistic effect between its highly polar polyamide backbone and aromatic side chains enables strong interactions with and subsequent disruption of the interfacial film composed of asphaltenes, resins, and other native surfactants (Fig. 10(c)). Finally, the synergy between the highly polar amide backbone and the aromatic side chains enables the demulsifier to effectively interact with, displace, and disrupt the interfacial film, thereby initiating rapid droplet coalescence and significantly accelerating emulsion separation (Fig. 10(d)).

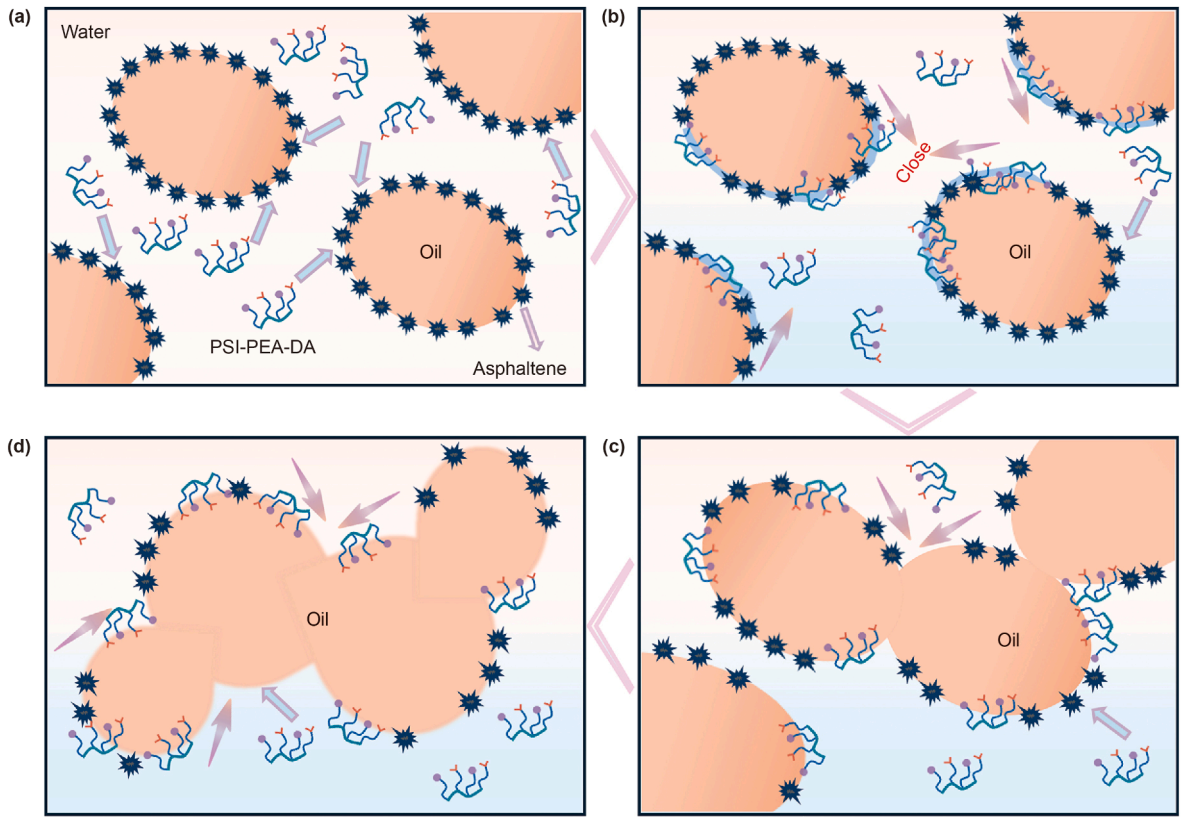

Fig. 10. Schematic diagram illustrating the demulsification process mediated by PSI-PEA-DA.

4. Conclusions

In this study, a strongly polar polyaspartamide-based oil-in-water (O/W) demulsifier was developed via the aminolysis of PSI. Bottle tests indicated that the co-grafted PSI-PEA-DA, containing both aromatic and alkyl side chains, exhibited superior oil separation capability and effectively separate 1.0 to 20.0 wt% O/W emulsions under identical conditions, outperforming PSI-DA. In contrast, PSI-PEA, modified exclusively with an aromatic side chain, tended to form hydrophilic micelles within O/W emulsions, resulting in a loss of interfacial activity and demulsification capability. Furthermore, static scale inhibition tests demonstrated that PSI-PEA-DA effectively prevented calcium sulfate deposition, achieving a scale inhibition efficiency of up to 84.5%. Mechanistic investigations reveal that the stronger polarity of the polyamide backbone in polyaspartamide-based demulsifiers enables effective separation of O/W emulsions at low temperatures. Moreover, the incorporation of an aromatic side chain enhances the interfacial activity of PSI-PEA-DA, strengthening its interaction with asphaltene and improving its ability to solubilize and disrupt the oil–water interface, as well as to promote flocculation and coagulation processes. In summary, this study demonstrates that increasing aromaticity and polarity are effective strategies for developing high-performance demulsifiers suitable for low-temperature applications. However, due to their amphiphilic nature, demulsifiers can adjust their dispersion state in response to varying environmental conditions. Therefore, when designing novel low-temperature demulsifiers, it is essential not only to regulate aromatic content and polarity but also to rationally design the molecular structure to prevent changes in dispersion behavior that could compromise demulsification and flocculation performance.

CRediT authorship contribution statement

Xiao-Hong Li: Writing – original draft, Supervision, Investigation. **Xun Xie:** Writing – original draft, Investigation, Data curation. **Xia Liu:** Methodology, Investigation. **Lan Zhou:** Investigation, Formal analysis. **Huan-Jiang Wang:** Writing – review & editing, Funding acquisition, Formal analysis. **Can Cui:** Methodology, Conceptualization. **Ya-Dian Xie:** Resources, Project administration, Methodology.

Data availability

Data will be made available on request.

Declaration of competing interest

The authors declare that they have no known competing financial interests or personal relationships that could have appeared to influence the work reported in this paper.

Acknowledgments

This research was funded by the National Natural Science Foundation of China (No. 22262008), Guizhou Provincial Basic Research Program (Natural Science) (No. [2024] 503), Guizhou Provincial Engineering Research Center for Low-dimensional Materials and Applications, Environmental Science and Technology Project of Department of Ecology and Environment of Guizhou Province (No. GZSJCZX2024142), Natural Science Foundation Research Project of Guizhou Minzu University (No. GZMU [2023] YB15), the Science and Technology Innovation Talent Team Construction Project (No. CXTD2025037), the Science and Technology

Support Program Project of Guizhou Province (No. 2025073), the Key Laboratory of Higher Education in Guizhou Province (No. 2022046), and Foundation Project of the "New Quality Frontier" Leading Project of Guizhou Association for Science and Technology (Nos. 2025XZQYXM-03-01, 2025XZQYXM-02-01).

Appendix A. Supplementary data

Supplementary data to this article can be found online at https://doi.org/10.1016/j.petsci.2026.05.014.

References

Al-Ghouti, M.A., Al-Kaabi, M.A., Ashfaq, M.Y., et al., 2019. Produced water characteristics, treatment and reuse: A review. J. Water Process Eng. 28, 222–239. https://doi.org/10.1016/j.jwpe.2019.02.001.

Al-Sakkaf, M.K., Onaizi, S.A., 2024. Effects of emulsification factors on the characteristics of crude oil emulsions stabilized by chemical and biosurfactants: A review. Fuel 361, 130604. https://doi.org/10.1016/j.fuel.2023.130604.

Cai, Y.-H., Zhao, J.-L., Guo, X.-Y., et al., 2022. Synthesis of polyaspartic acid-capped 2-aminoethylamino acid as a green water treatment agent and study of its inhibition performance and mechanism for calcium scales. RSC Adv. 12, 24596–24606. https://doi.org/10.1039/d2ra04075a.

Chen, H., Xu, W., Chen, T., et al., 2005. Aggregation of biodegradable amphiphilic poly(succinimide-*co*-*N*-propyl aspartamide) and poly(*N*-dodecyl aspartamide-*co*-*N*-propyl aspartamide) in aqueous medium and its preliminary drug-released properties. Polymer 46, 1821–1827. https://doi.org/10.1016/j.polymer.2004.12.042.

Chen, J., Xu, L., Han, J., et al., 2015. Synthesis of modified polyaspartic acid and evaluation of its scale inhibition and dispersion capacity. Desalination 358, 42–48. https://doi.org/10.1016/j.desal.2014.11.010.

Chen, Y., Tian, G., Liang, H., et al., 2019. Synthesis of magnetically responsive hyperbranched polyamidoamine based on the graphene oxide: Application as demulsifier for oil-in-water emulsions. Int. J. Energy Res. 43, 4756–4765. https://doi.org/10.1002/er.4614.

Deng, J., Zhang, X., Gu, Z., et al., 2025. High-efficiency purification of alkali-surfactant-polymer flooding produced water by ultrasonication-ionic liquids combination: Performance and separation mechanism. Sep. Purif. Technol. 363, 132255. https://doi.org/10.1016/j.seppur.2025.132255.

Galano, A., Alvarez-Idaboy, J.R., 2006. A new approach to counterpoise correction to BSSE. J. Comput. Chem. 27 (11), 1203–1210. https://doi.org/10.1002/jcc.20438.

Griffin, W.C., 1954. Calculation of HLB values of non-ionic surfactants. J. Soc. Cosmet. Chem. 5, 249–256.

Hao, H., Qi, X., Tang, W., et al., 2021. Energy decomposition analysis reveals the nature of lone pair–π interactions with cationic π systems in catalytic acyl transfer reactions. Org. Lett. 23 (11), 4411–4414. https://doi.org/10.1021/acs.orglett.1c01351.

Hassanshahi, N., Hu, G., Li, J., 2020. Application of ionic liquids for chemical demulsification: A review. Molecules 25, 4915. https://doi.org/10.3390/molecules25214915.

Huang, Y., Qiao, C., Li, Z., et al., 2025. Mechanistic insights into the role of branched polyethylenimine in breaking asphaltene-stabilized oil-in-water emulsions: Temperature effects. Sep. Purif. Technol. 362, 131913. https://doi.org/10.1016/j.seppur.2025.131913.

Husain, A., Al-Harthi, M.A., 2023. Chemical treatment of oilfield wastewater and the effect of temperature on treatment efficiency: A review. J. Pet. Sci. Eng. 220, 111089. https://doi.org/10.1016/j.petrol.2022.111089.

Kuang, J., Jiang, X., Mi, Y., et al., 2019. Demulsification of oil-in-water emulsions using hyperbranched poly(amido amine) demulsifiers with 4,4-diaminodiphenyl methane as initial cores. J. Appl. Polym. Sci. 137, 48846. https://doi.org/10.1002/app.48846.

Lam, D.-L., Cheng, Y.-T., Huang, C.-J., 2023. Biodegradable and pH-responsive amphiphilic poly(succinimide) derivatives for triggered release of antibiotics for management of infected wounds. ACS Appl. Mater. Interfaces 15, 53297–53309. https://doi.org/10.1021/acsami.3c12939.

Lee, J., Babadagli, T., 2020. Comprehensive review on heavy-oil emulsions: Colloid science and practical applications. Chem. Eng. Sci. 228, 115962. https://doi.org/10.1016/j.ces.2020.115962.

Lei, M., Huang, H., Liu, J., et al., 2023. A gemini ionic liquid and its low-temperature demulsification performance in water-in-crude oil emulsions. Colloids Surf. A Physicochem. Eng. Aspects 671, 131696. https://doi.org/10.1016/j.colsurfa.2023.131696.

Li, Z., Geng, H., Wang, X., et al., 2018. Noval tannic acid-based polyether as an effective demulsifier for water-in-aging crude oil emulsions. Chem. Eng. J. 354, 1110–1119. https://doi.org/10.1016/j.cej.2018.08.117.

Liu, Z., Lu, T., Chen, Q., 2021. Intermolecular interaction characteristics of the all-carboatomic ring, cyclo[18]carbon: Focusing on molecular adsorption and stacking. Carbon 171, 514–523. https://doi.org/10.1016/j.carbon.2020.09.048.

Low, J.Y., Khe, C.S., Usman, F., et al., 2024. Review on demulsification techniques for oil/water emulsion: Comparison of recyclable and irretrievable approaches. Environ. Res. 243, 117840. https://doi.org/10.1016/j.envres.2023.117840.

Lu, T. Molclus program, *Version* 1.9.9.9. http://www.keinsci.com/research/molclus.html (Accessed September 20, 2025).

Lu, T., 2024. Theoretical prediction and comprehensive characterization of an all-nitrogenatomic ring, cyclo[18]nitrogen (N_{18}). ChemPhysChem 25 (16), e202400377. https://doi.org/10.1002/cphc.202400377.

Lu, T., Chen, F., 2012. Multiwfn: A multifunctional wavefunction analyzer. J. Comput. Chem. 33 (5), 580–592. https://doi.org/10.1002/jcc.22885.

Lü, T., Qi, D., Zhang, D., et al., 2018. Facile synthesis of *N*-(aminoethyl)-aminopropyl functionalized core-shell magnetic nanoparticles for emulsified oil-water separation. J. Alloys Compd. 769, 858–865. https://doi.org/10.1016/j.jallcom.2018.08.071.

Ma, J., Li, X., Zhang, X., et al., 2020. A novel oxygen-containing demulsifier for efficient breaking of water-in-oil emulsions. Chem. Eng. J. 385, 123826. https://doi.org/10.1016/j.cej.2019.123826.

Ma, J., Yang, Y., Li, X., et al., 2021. Mechanisms on the stability and instability of water-in-oil emulsion stabilized by interfacially active asphaltenes: Role of hydrogen bonding reconstructing. Fuel 297, 120763. https://doi.org/10.1016/j.fuel.2021.120763.

Mi, Y., Shen, L., Huang, X., et al., 2025. Synthesis of an efficient demulsifier derived from cotton cellulose and its demulsification performance in oily wastewater. Int. J. Biol. Macromol. 296, 139839. https://doi.org/10.1016/j.ijbiomac.2025.139839.

Mooibroek, T.J., Gamez, P., Reedijk, J., 2008. Lone pair–π interactions: A new supramolecular bond? CrystEngComm 10 (11), 1501. https://doi.org/10.1039/b812026a.

Neese, F., Wennmohs, F., Becker, U., et al., 2020. The ORCA quantum chemistry program package. J. Chem. Phys. 152 (22), 224108. https://doi.org/10.1063/5.0004608.

Olajire, A.A., 2014. Review of ASP EOR (alkaline surfactant polymer enhanced oil recovery) technology in the petroleum industry: Prospects and challenges. Energy 77, 963–982. https://doi.org/10.1016/j.energy.2014.09.005.

Onaizi, S.A., 2022. Effect of salinity on the characteristics, pH-triggered demulsification and rheology of crude oil/water nanoemulsions. Sep. Purif. Technol. 281, 119956. https://doi.org/10.1016/j.seppur.2021.119956.

Raya, S.A., Mohd Saaid, I., Abbas Ahmed, A., et al., 2020. A critical review of development and demulsification mechanisms of crude oil emulsion in the petroleum industry. J. Pet. Explor. Prod. Technol. 10 (4), 1711–1728. https://doi.org/10.1007/s13202-020-00830-7.

Ruidas, S., Das, A., Kumar, S., et al., 2022. Non-fluorinated and robust superhydrophobic modification on covalent organic framework for crude-oil-in-water emulsion separation. Angew. Chim. Int. Ed. 61 (41), e202210507. https://doi.org/10.1002/anie.202210507.

Shen, L., Ai, G., Liu, H., et al., 2024. Synthesis and demulsification performance of a novel low-temperature demulsifier based on trimethyl citrate. J. Hazard. Mater. 472, 134543. https://doi.org/10.1016/j.jhazmat.2024.134543.

Sousa, A.M., Matos, H.A., Pereira, M.J., 2022. Properties of crude oil-in-water and water-in-crude oil emulsions: A critical review. Ind. Eng. Chem. Res. 61 (1), 1–20. https://doi.org/10.1021/acs.iecr.1c02744.

Sun, H., Wang, Q., Li, X., et al., 2020. Novel polyether-polyquaternium copolymer as an effective reverse demulsifier for O/W emulsions: Demulsification performance and mechanism. Fuel 263, 116770. https://doi.org/10.1016/j.fuel.2019.116770.

Tang, L., Wang, T., Xu, Y., et al., 2024. Research and application progress of crude oil demulsification technology. Processes 12 (10), 2292. https://doi.org/10.3390/pr12102292.

Vafajoo, L., Ganjian, K., Fattahi, M., 2012. Influence of key parameters on crude oil desalting: An experimental and theoretical study. J. Pet. Sci. Eng. 90 (91), 107–111. https://doi.org/10.1016/j.petrol.2012.04.022.

Velazco-de-la-Garza, J., Avérous, L., de Jesús Sosa-Santillán, G., et al., 2020. Biological properties of novel polysuccinimide derivatives synthesized *via* quaternary ammonium grafting. Eur. Polym. J. 131, 109705. https://doi.org/10.1016/j.eurpolymj.2020.109705.

Wan, H., Ye, F., Wang, J., et al., 2025. Low-temperature demulsification of pectinate alternating copolymer and its mechanism. Fuel 390, 134726. https://doi.org/10.1016/j.fuel.2025.134726.

Wang, D., Yang, D., Huang, C., et al., 2021. Stabilization mechanism and chemical demulsification of water-in-oil and oil-in-water emulsions in petroleum industry: A review. Fuel 286, 119390. https://doi.org/10.1016/j.fuel.2020.119390.

Wang, G., Xiao, Y., Xu, H., et al., 2018. Development of multifunctional avermectin poly(succinimide) nanoparticles to improve bioactivity and transportation in rice. J. Agric. Food Chem. 66 (43), 11244–11253. https://doi.org/10.1021/acs.jafc.8b03295.

Wang, H., Liu, J., Xu, H., et al., 2016. Demulsification of heavy oil-in-water emulsions by reduced graphene oxide nanosheets. RSC Adv. 6 (108), 106297–106307. https://doi.org/10.1039/c6ra18898b.

Wang, H., Wu, Y., Wu, Z., et al., 2024. Preparation of a low-temperature poly (amino acids) demulsifier and its demulsification mechanism. Fuel 365, 131237. https://doi.org/10.1016/j.fuel.2024.131237.

Wang, H., Xu, H., Jia, W., et al., 2017. Revealing the intermolecular interactions of asphaltene dimers by quantum chemical calculations. Energy Fuels 31 (3), 2488–2495. https://doi.org/10.1021/acs.energyfuels.6b02738.

Wu, J., Yan, F., Jia, Q., et al., 2021. QSPR for predicting the hydrophile-lipophile balance (HLB) of non-ionic surfactants. Colloids Surf. A Physicochem. Eng. Aspects 611, 125812. https://doi.org/10.1016/j.colsurfa.2020.125812.

Wu, Z., Yang, Q., Cui, C., et al., 2024. Aromatic poly (amino acids) as an effective low-temperature demulsifier for treating crude oil-in-water emulsions. J. Hazard. Mater. 472, 134608. https://doi.org/10.1016/j.jhazmat.2024.134608.

Yan, S., Yuan, Z., Qian, H., et al., 2024. Advanced magnetic nanospheres for oil pollutant management: Dual roles in emulsification and demulsification. J. Hazard. Mater. 480, 136026. https://doi.org/10.1016/j.jhazmat.2024.136026.

Wu, Y., Zhang, D., Ma, P., et al., 2018. Lithium hexamethyldisilazide initiated superfast ring opening polymerization of alpha-amino acid N-carboxyanhydrides. Nat. Commun. 9, 9257. https://doi.org/10.1038/s41467-018-07711-y.

Yan, S., Jiang, P., Zhang, X., et al., 2025. Advancing oil-water separation: Design and efficiency of amphiphilic hyperbranched demulsifiers. J. Colloid Interface Sci. 677, 583–596. https://doi.org/10.1016/j.jcis.2024.08.101.

Yang, X., Chen, S., Chen, H., et al., 2025. Comprehensive review of stabilising factors, demulsification methods, and chemical demulsifiers of oil-water emulsions. Sep. Purif. Technol. 358, 130206. https://doi.org/10.1016/j.seppur.2024.130206.

Yeh, J.-C., Yang, H.-H., Hsu, Y.-T., et al., 2013. Synthesis and characteristics of biodegradable and temperature responsive polymeric micelles based on poly(aspartic acid)-g-poly(N-isopropylacrylamide-co-N,N-dimethylacrylamide). Colloids Surf. A 421, 1–8. https://doi.org/10.1016/j.colsurfa.2012.12.014.

Yonguep, E., Kapiamba, K.F., Kabamba, K.J., et al., 2022. Formation, stabilization and chemical demulsification of crude oil-in-water emulsions: A review. Pet. Res. 7 (4), 459–472. https://doi.org/10.1016/j.ptlrs.2022.01.007.

Yu, X., Wang, J., Ye, F., 2024. Cyclodextrin decorated with quaternary ammonium salt and hydrophobic chain as green demulsifier for the demulsification of oily wastewater. J. Mol. Liq. 406, 125100. https://doi.org/10.1016/j.molliq.2024.125100.

Zhang, S., Qu, H., Yang, Z., et al., 2017. Scale inhibition performance and mechanism of sulfamic/amino acids modified polyaspartic acid against calcium sulfate. Desalination 419, 152–159. https://doi.org/10.1016/j.desal.2017.06.016.

Zhang, X., He, C., Mostafa, M.Y.M., et al., 2025a. Constructing oxygen-based multiple hydrogen bonding sites and delocalized π bonds for efficient oil-water-solid interfacial separation. J. Hazard. Mater. 490, 137766. https://doi.org/10.1016/j.jhazmat.2025.137766.

Zhang, X., Muhmmad Mostafa, M.Y., Wang, Z., et al., 2025b. Efficient dewatering of water-in-shale oil emulsions by a newly branched demulsifier co-modified by phenoxy and carboxyl. Sep. Purif. Technol. 373, 133553. https://doi.org/10.1016/j.seppur.2025.133553.

Zhang, Z., Feng, X., Zeng, G., et al., 2021. Hyperbranched poly(amido amine) demulsifiers using diaminonaphthalene as the central core and their demulsification performance in oil-in-water and water-in-oil emulsions. Energy Fuels 35 (4), 3095–3103. https://doi.org/10.1021/acs.energyfuels.0c03912.

Zolfaghari, R., Fakhru'l-Razi, A., Abdullah, L.C., et al., 2016. Demulsification techniques of water-in-oil and oil-in-water emulsions in petroleum industry. Sep. Purif. Technol. 170, 377–407. https://doi.org/10.1016/j.seppur.2016.06.026.